Strathprints Institutional Repository

Optical control of scattering, absorption and lineshape in nanoparticles

Benjamin Hourahine and Francesco Papoff*

SUPA, Department of Physics, University of Strathclyde, 107 Rottenrow, Glasgow G4 0NG, UK.

*f.papoff@strath.ac.uk

Abstract: We find exact conditions for the enhancement or suppression of internal and/or scattered fields in any smooth particle and the determination of their spatial distribution or angular momentum through the combination of simple fields. The incident fields can be generated by a single monochromatic or broad band light source, or by several sources, which may also be impurities embedded in the nanoparticle. We can design the lineshape of a particle introducing very narrow features in its spectral response.

OCIS codes: (290.0290) Scattering; (020.3690) Line shapes and shifts; (160.4236) Nanomaterials; (290.5825) Scattering theory.

References and links

1. M. Abb, P. Albella, J. Aizpurua, and O. Muskens, "All-optical control of a single plasmonic nanoantenna-ITO hybrid," Nano Lett. **11**, 2457–2463 (2011).
2. A. Kubo, K. Onda, H. Petek, Z. Sun, Y. Jung, and H. Kim, "Femtosecond imaging of surface plasmon dynamics in a nanostructured silver film," Nano Lett. **5**, 1123–1127 (2005).
3. M. Durach, A. Rusina, and M. Stockman, "Full spatiotemporal control on the nanoscale," Nano Lett. **7**, 3145–3149 (2007).
4. M. Martin Aeschlimann, M. Bauer, D. Bayer, T. Tobias Brixner, F. Garcıa de Abajo, W. Pfeiffer, M. Rohmer, C. Spindler, and F. Felix Steeb, "Adaptive subwavelength control of nano-optical fields," Nature **446**, 301–304 (2007).
5. H. Noh, Y. Chomg, A. Stone, and H. Cao, "Perfect coupling of light to surface plasmons by coherent absorption," Phys. Rev. Lett. **108**, 186805 (2012).
6. R. Pierrat, C. Vandenbem, M. Fink, and R. Carminati, "Subwavelength focusing inside an open disordered medium by time reversal at a single point antenna," Phys. Rev. A **87**, 041801 (2013).
7. J. Jeffers, "Interference and the lossless lossy beam splitter," Journ. Mod. Opt. **47**, 1819–1824 (2000).
8. J. Zhang, K. MacDonald, and N. Zheludev, "Controlling light-with-light without nonlinearity," Light: Science & Appl. **1**, e18 (2012).
9. M. Mazilu, J. Baumgartl, S. Kosmeier, and K. Dholakia, "Optical eigenmodes; exploiting the quadratic nature of the energy flux and of scattering interactions," Opt. Express **19**, 933–945 (2011).
10. F. Papoff and B. Hourahine, "Geometrical mie theory for resonances in nanoparticles of any shape," Opt.Express **19**, 21432–21444 (2011).
11. M. Doherty, A. Murphy, R. Pollard, and P. Dawson, "Surface-enhanced raman scattering from metallic nanostructures: Bridging the gap between the near-field and far-field responses," Phys. Rev. X **3**, 011001 (2013).
12. P. C. Waterman, "The T-matrix revisited," JOSA A **24**, 2257–2267 (2007).
13. P. Barber and C. Yeh, "Scattering of electromagnetic waves by arbitrarily shaped dielectric bodies," Appl. Opt. **14**, 2864–2872 (1975).
14. M.I.Mishchenko, J. H. Hovernier, and L. D. Travis, eds., *Light Scattering by Nonspherical Particles: Theory, Measurements and Applications* (Academic Press, 2000).
15. A. Taflove, *Computational Electrodynamics: The Finite Difference Time-Domain Method* (Artech House Publishers, Boston, MA, 1995).
16. R. Rodríguez-Oliveros and J. A. Sánchez-Gil, "Localized surface-plasmon resonances on single and coupled nanoparticles through surface integral equations for flexible surfaces," Opt. Express **19**, 12208–12219 (2011).

#192195 - $15.00 USD Received 12 Jun 2013; revised 9 Aug 2013; accepted 13 Aug 2013; published 22 Aug 2013

17. B. F. Farrell and P. J. Ioannou, "Generalized stability theory. part i: Autonomous operators," Journ. of Atm. Sc. **53**, 2025–2040 (1996).
18. J. A. Stratton and L. J. Chu, "Scattering of light from a two-dimensional array of spherical particles on a substrate," Phys. Rev. **56**, 99–107 (1939).
19. I. Malitson, "Interspecimen comparison of the refractive index of fused silica," Journal of the Optical Society of America **55**, 1205–1209 (1965).
20. H. Wei, X. Xue, J. Leach, M. J. Padgett, S. M. Barnett, S. Franke-Arnold, and a. J. C. E. Yao, "Simplified measurement of the orbital angular momentum of photons," Opt. Commun. **223**, 117–122 (2003).
21. K. Holms, B. Hourahine, and F. Papoff, "Calculation of internal and scattered fields of axisymmetric nanoparticles at any point in space," J. Opt. A: Pure Appl. Opt. **11**, 054009 (2009).
22. T. Rother, M. Kahnert, A. Doicu, and J. Wauer, "Surface Green's Function of the Helmholtz Equation in Spherical Coordinates," Prog. Electromag. Res. **38**, 47–95 (2002).
23. E. Hannan, "The general theory of canonical correlation and its relation to functional analysis," J. Aust. Math. Soc. **2**, 229–242 (1961/1962).
24. A. Knyazev, A. Jujusnashvili, and M. Argentati, "Angles between Infinite Dimensional Subspaces with Applications to the Rayleigh-Ritz and Alternating Projectors Methods," Journ. of Func. Analys. **259**, 1323–1345 (2010).
25. W. J. Firth and A. Yao, "Giant excess noise and transient gain in misaligned laser cavities," Phys. Rev. Lett. **95**, 073903 (2005).
26. F. Papoff, G. D'Alessandro, and G.-L. Oppo, "State dependent pseudoresonances and excess noise," Phys. Rev. Lett. **100**, 123905 (2008).
27. F. Papoff and G. Robb, "Rapid coherent optical modulation of atomic momenta via pseudoresonances," Phys. Rev. Lett. **108**, 113902 (2012).
28. A. Doicu, Y. Eremin, and T. Wreidt, *Acoustic and Electromagnetic Scattering Analysis Using Discrete Sources* (Accademic Press, 2000).

Introduction

Control of near and far field optical emission and the optimization of coupling between incident light and nanostructures are fundamental issues that underpin the ability to enhance sub-wavelength linear and nonlinear light-matter interaction processes in nanophotonics. Nonlinear [1] and linear control based on pulse shaping [2, 3], combination of adaptive feedbacks and learning algorithms [4], as well as optimization of coupling through coherent absorption [5] and time reversal [6] have all been recently investigated. Interference between fields was some time ago proposed in quantum optics as a way to suppress losses in lossy beam splitter [7] and has been recently applied to show control of light with light in linear plasmonic metamaterials [8]. In paraxial optics, modes have been used for optical control [9].

In this paper we develop a general analytical theory for the control of the modes of scattered and internal fields in nanostructures of any shape and at any frequency which allow us to either enhance or suppress internal and/or scattered fields and determine their spatial distribution or angular momentum. Most importantly, we can design the lineshape of the particle and introduce very narrow features in its spectral response. This method requires varying the relative amplitudes and phases of $N+1$ incident fields in order to control N channels. Modes of the internal and scattered fields of nanoparticles are coupled pairwise, each pair forming an interaction channel for the incident light [10]. Some of the scattering modes efficiently transport energy into the far field, while others are mostly limited to the near field region around their nanostructure [11]. Depending on the channels involved, it is possible to determine the flow of energy outside the particle by controlling the scattered field in the far and/or in the near field regions, or the absorption of energy by the particle through controlling the amplitude of the internal field. The incident fields considered here are commonly available in experiments and can be monochromatic or broad band. A practical implementation requires simply the control of the relative phases of incident fields and can be achieved using only one source of light together with beam splitters and phase modulators, or a mixture of sources, which may also be impurities embedded in the nanoparticle, such as atoms, molecules or quantum dots. We provide simple sketches of experimental set-ups suitable to implement our theory in Fig. 1. The coherence

#192195 - $15.00 USD Received 12 Jun 2013; revised 9 Aug 2013; accepted 13 Aug 2013; published 22 Aug 2013

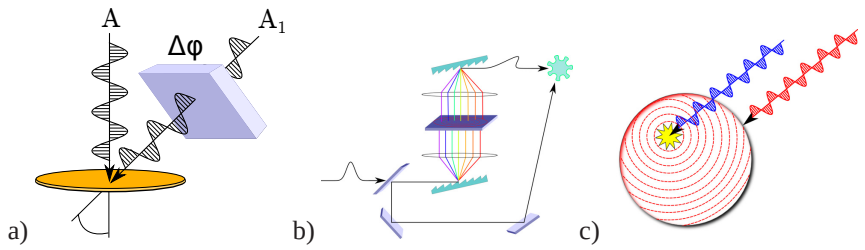

Fig. 1. Suggested experimental geometries for control of optical channels. a) Monochromatic incident light fields approaching a disc shaped nanostructure to change the amplitudes of a specified principal mode, two independent light sources with amplitudes A and A_1 and a specified relative phase $\Delta\Phi$ are used. b) A more general spatial-light modulator approach for changing phase and/or amplitude over a range of wavelengths for a broadband source or an applied pulse of light. Here the incident light is split into two paths, with one being dispersed and its complex amplitude modified as a function of wavelenth, before being re-combined and applied to the nanostructure together with the light which followed the second path. c) Generation of phase controlled light from an internal source within a nano-particle or nanostructure. This is driven by the blue by incident light, and re-radiates through a coherent process, such as two photon decay or parametric down conversion, in the red. This then interacts with external light incident at the emission wavelength (again in red). By exchanging the roles of the red and blue light sources, the same scheme can be used for control in the context of second harmonic generation.

length of such sources has to be of the order of the size of the particle, so even conventional lamps may be used in some applications, as long as the difference between the optical paths from the sources to the particle is within the coherence length. The internal sources may emit radiation at the frequency under control not only through elastic scattering, but also through inelastic scattering and nonlinear processes such as harmonic generation and amplification of light at the nanoscale. Therefore our approach can be used to also optically control non-linear processes. In the following we briefly review the theory of internal and scattering modes for smooth particles, then derive the control conditions for fields at the surface of a particle, consider the types of light sources able to implement those conditions and show some numerical illustrations of these ideas. We also show that a simple parameter scan is sufficient to find optimal control conditions even without a detailed knowledge of the modes of the particles, as it is the case in most practical applications.

Theory

In this section we derive an analytical theory of control of the optical response of non-spherical metallic and dielectric nanoparticles without sharp edges with light. Several efficient techniques have been developed to study scattering in non spherical particles [12, 13, 14, 15, 16]; our work is based on a recent generalization of Mie theory [10] that allows us to expand internal and scattered fields in terms of the intrinsic modes of the particle. These modes and the property that the projection on the surface of the particle of each scattering mode, $\{s_n\}$, is spatially correlated to the projection of only *one* internal mode, $\{i_n\}$, and vice versa, are essential to derive analytical conditions for optical control of optical properties. We recall that the spatial correlation of two modes is defined by an integral over the particle surface for the scalar product of their projections. These spatial correlations can be interpreted geometrically by introducing the principal cosines $i_n \cdot s_n = \cos(\xi_n)$. The principal vectors, their coefficients $\{a^{i,s}\}$ and correlations depend on the wavelength parametrically through the frequency dependence of the

#192195 - $15.00 USD Received 12 Jun 2013; revised 9 Aug 2013; accepted 13 Aug 2013; published 22 Aug 2013

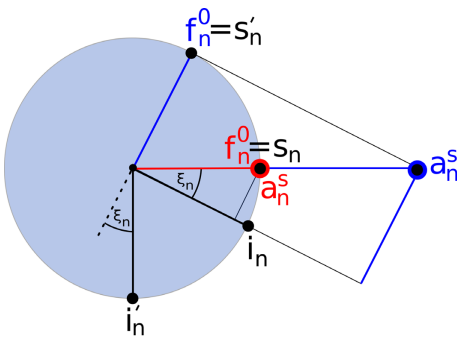

Fig. 2. Schematic of one pair of principal modes of a nanostructure interacting with different incident fields. The modes and incident fields have been normalized to unit magnitude (the marked circle). The amplitude, a_n^s, of the scattered mode, s_n, is given by the intersection of straight lines parallel to i_n and passing through the extrema of the incident field and a line containing s_n. From this construction, we can see that a unit magnitude field with f_n parallel to s_n induces amplitudes $a_n^s = 1$, $a_n^i = 0$ (shown in red, corresponding to Eq. (1)), while a unit field with f_n parallel to s'_n (and orthogonal to i_n) induces the largest amplitude possible a_n^s from a unit magnitude incident field along with a non-vanishing internal amplitude a_n^i (blue, matching Eq. (2)). Equivalently [17], the amplitudes are proportional to the scalar products of the incident field with the biorthogonal modes $\{i'_n\}$ and $\{s'_n\}$, as shown in Eq. (6).

dielectric and magnetic permittivity and permeability [10]. The relative orientation of the n^{th} set of principal modes and their related biorthogonal modes, $\{i'_n\}$ and $\{s'_n\}$, allows us to find the amplitudes a_n^i, a_n^s for any incident field, see Appendix Eqs. (6) and (7). These are shown schematically in Fig. 2.

The geometrical meaning of the spatial correlations enables us to use the geometry of a non-orthogonal basis of vectors [17] to determine the surface fields which excite s_n but not i_n (or i_n and not s_n), or that produce the largest amplitude for modes s_n or i_n (see Fig. 2). We recall that any incident field can be decomposed as $f = f_n + f_{n_\perp}$, with f_n the part of the incident field that couples only with the n^{th} modes and $f_{n_\perp}$ being the part that does not. We find that

$$f_n = s_n \rightarrow a_n^s = 1,\ a_n^i = 0, \tag{1}$$

$$f_n = s'_n \rightarrow a_n^s = \frac{1}{\sin(\xi_n)},\ a_n^i = -\frac{\cos(\xi_n)}{\sin(\xi_n)}. \tag{2}$$

Eq. (1) give the requirement for incident fields that, irrespectively of $f_{n_\perp}$, produce excitation of only the scattering mode, i.e., null amplitude for the corresponding internal mode. Alternatively the largest amplitude of the scattering mode is obtained for fields with the form of Eq. (2). Note that we are considering only incident fields with $f_n \cdot f_n = 1$ in Eqs. (1,2) to avoid trivial effects due to the overall amplitude of the incident fields. Figure 2 depicts the corresponding incident fields and the associated amplitudes of the scattered light in mode s_n for both types of incident field. The analogous conditions for i_n are found by exchanging s with i in Eqs. (1, 2).

Two points are worth noting. First, these are exact conditions for the surface fields that are valid at any frequency and have two possible applications: control of a mode (or modes) over a range of frequency and introduction of narrow band features in the spectral response of the particle. Second, the largest amplitude for a mode is not achieved through single mode excitation, but by an optimal excitation that produces amplitudes in the two principal modes of the channel. For physical applications it is necessary to generate incident fields which have tangent

#192195 - $15.00 USD Received 12 Jun 2013; revised 9 Aug 2013; accepted 13 Aug 2013; published 22 Aug 2013

components that fulfill Eqs. (1), or (2). The case $f = s_n$ can be in principle realized through time reversal of the lasing mode of an amplifier with the same shape as the particle and gain opposite to the loss [5] at the resonant frequency of the mode. To experimentally realize this is quite challenging, as radiation would need to converge towards the particle from all directions. We are instead interested in deriving general conditions for optimal excitation of modes at any frequency with easily accessible sources of radiation. In general, an incident field $F(\mathbf{r})$ with tangent components $f = i_n$ or $f = s_n$ cannot be realized using common sources of radiation external to the particle, such as laser beams or SNOM tips, or even internal sources such as fluorescent or active hosts. This is because these sources emit waves that are neither outgoing radiating waves in the external medium, as is the scattering mode, s_n, nor standing waves in the internal medium, such as the internal mode, i_n. However, by combining two or more of these sources with appropriate phases and amplitudes, it is possible to control in a simple and effective way the few dominant interaction channels of any nanoparticle. To construct fields to realize the conditions of Eqs. (1) or (2) requires two linearly independent incident fields, Af, and $A_1 f^1$, both coupled to the channel n, such that

$$\frac{s_n \cdot f}{s_n \cdot f^1} \neq \frac{i_n \cdot f}{i_n \cdot f^1}. \tag{3}$$

The condition for the suppression of i_n is

$$A_1 = -A\frac{i_n \cdot f}{i_n \cdot f^1}, \tag{4}$$

while condition for maximal excitation of s_n for incident light such that $|A_1 f_1 + Af|$ is constant (the radius of the circle in Fig. 2) becomes

$$A_1 = -A\frac{i_n' \cdot f}{i_n' \cdot f^1}, \tag{5}$$

with A, A_1 being complex amplitudes that can be experimentally adjusted through phase plates and dicroic elements (Fig. 1 suggests a geometry for constructing these fields, while a numerical example of scanning the relative complex amplitude to produce specific scattered light is shown later). Analogous conditions for optimization of i_n and suppression of s_n can be found by swapping i_n, i_n' with s_n, s_n' in Eqs. (4, 5): the generalization of Eq. (4) to a larger number of modes is presented in the Appendix.

We note that conservation of energy applies to the incident scattered and internal fields, but not necessarily to each interaction channel separately. However, if incident fields with $f_n \neq 0, f_{n_\perp} = 0$ exist, the conservation of energy applies to the n channel. From the Stratton-Chu representations [18] (see Appendix) we can show that in particles where the dependence of the electric (and magnetic) parts of i_n, s_n, f_n on the surface coordinates is the same, such as for sphere and infinite cylinders, the ratios in Eq. (3) depends on the flux of energy of the incident field into the particle, and Eq. (3) is *always* violated when the sources are both either outside or inside the particle. For instance, in the case of a sphere any external source can be expanded by the set of regular multipoles with angular indexes l, m, while any internal source is expanded by the set of radiating spherical multipoles, as shown in the Appendix. In this case the amplitudes of internal and scattering modes cannot be controlled by independent external – or internal – sources: Eqs. (4, 5) become equivalent and lead to the simultaneous suppression of both i_n and s_n, while the maximization of the amplitudes of both scattering and internal modes is provided by ensuring that the contributions of the incident fields to the amplitudes add in phase. However, the condition for maximal excitation, Eq. (4), or suppression of a mode, Eq. (5), can be fulfilled also for spheres at any frequency provided one incident field is generated by an external source

#192195 - $15.00 USD Received 12 Jun 2013; revised 9 Aug 2013; accepted 13 Aug 2013; published 22 Aug 2013

and the other by an internal source, or that one incident field is a regular wave with with a power flow of $W_n = 0$ and the other an incoming wave with $W_n \neq 0$. Examples of internal sources important for applications are impurities scattering light inelastically at the same frequency as the external control beam or active centers excited non-radiatively. Incoming waves are more difficult to realize, but could be in principle obtained through time reversal techniques [6].

Applications

We now show numerically how the theory developed here can be applied. In Fig. 3 we show how we can suppress either the scattered or the internal mode of the resonant channel in a rounded rod-shaped glass-like particle. The height and the position of these curves, the "mode landscape" [10], are a property of the particle, but the specific amplitude of the modes which is color coded in the figure, depends also on the specific incident fields. For this example, the internal and scattered modes which reach resonance at ≈ 630 nm obey Eq. (3) for light from external sources, so can be independently addressed by suitable incident fields. Figures 3(a)–3(d) show the internal and scattered amplitudes for the modes of the particle due to two different linearly polarized plane wave light sources, while Figs. 3(e)–3(h) then show the result of forming combinations of these two incident fields such that amplitude of either the internal or the scattered part of the resonance is switched off, leaving the corresponding amplitude in the other space unchanged at the same values caused by the axially incident light. The same fixed combination of fields is used across the range of wavelengths shown, due to the relatively rapid change in phase of the principle modes, this leads to a fairly sharp "hole" in the amplitudes, in particular the internal modes (Fig. 3(e)).

In Fig. 4 we show how the angular momentum of the scattered light can be controlled for a gold disc, while also presenting a suggestion of how this might be performed experimentally. The disc has an electric dipole radiation pattern, leading to the far-field light scattering pattern and surface field shown in left sub-figure of Fig. 4(a) at its resonance at 697 nm. This resonance occurs in both the $m = \pm 1$ channels, where m is the eigenvalue of the angular momentum around the axis of the disc. Hence for simple plane polarized axial light, an equal linear mixture of both m channels results. However, a second plane-wave field which obeys the analogue of Eq. (3) for the scattering parts of the two different m-channel resonances, can be added to selectively cancel one or the other m-channel of the resonance. This leads to the middle sub-figure, where the square of the electric field in the vicinity of the particle and the scattering into the far field become close to cylindrically symmetric, consisting only of $m = +1$ light. Finally by introducing a third field, both m-channels of the resonance are no longer coupling to the incident light, leading to the loss of nearly all of the surface field and a weak scattering of light into the far field. The present $m = -1$ canceling case could be experimentally realized by, for example, the situation depicted in Figure 1(a) – this is a direct analogue to the theoretical configuration of the fields used in Fig. 4(a). In the absence of knowledge of the principal mode amplitudes that are caused by the incident fields, scanning the relative complex amplitude of the two light sources can be used to identify the conditions for removal of one mode. The left figure of 4(b) shows the scattering cross section from the disc as both the relative phase and amplitude are varied for the two fields. The minimum scattering occurs close to the point at which only one of the m channel resonances is active (the second sub-figure showing purely the light in the $m = +1$ channel), but to actually reach the exact condition requires monitoring the amount of the light coming from the desired principal mode (for example using the approach of [20]). The present example controls the field enhancement of a resonance in the $m = \pm 1$ channels, however, this approach also applies for other m channels and does not require a resonance to be present at the wavelength, only that relatively few modes dominate the interaction with incident light.

#192195 - $15.00 USD Received 12 Jun 2013; revised 9 Aug 2013; accepted 13 Aug 2013; published 22 Aug 2013

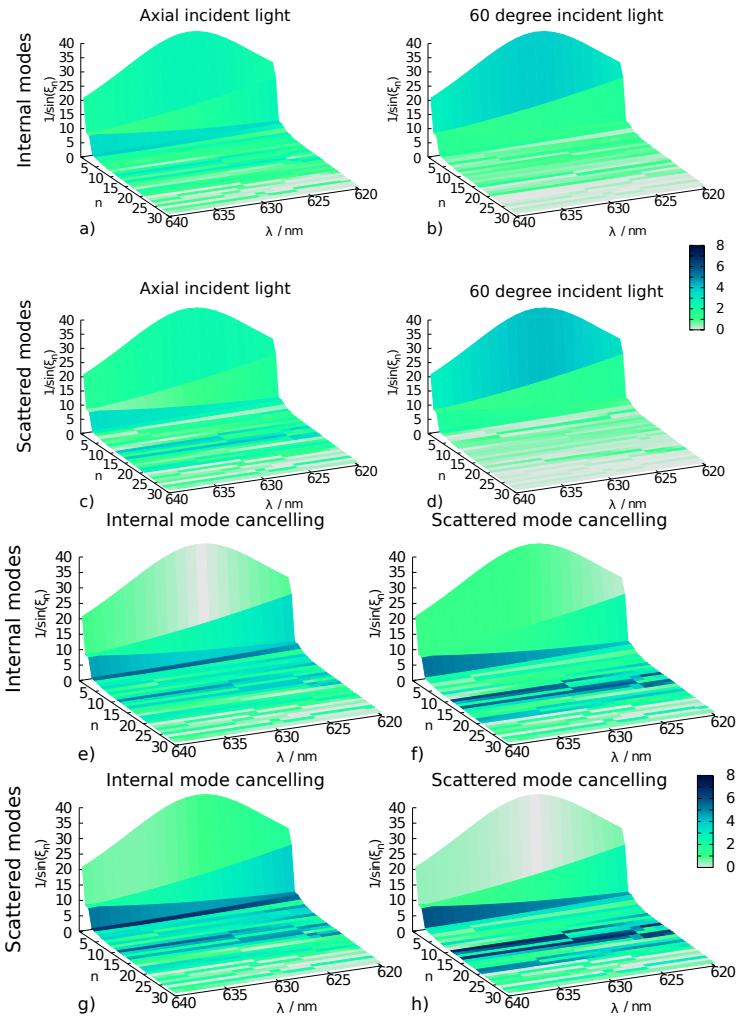

Fig. 3. Internal and scattered mode amplitudes of a rounded rod-shaped dielectric ($n = 1.5$) particle, of 2 μm length and 0.7 μm diameter around one of its (many) resonances at $\sim$ 630 *nm*. The height of this landscape is $\sin^{-1}(\xi)$, i.e. the largest value of amplitude possible for $|f_n| = 1$; while the shading of the traces overlaid on top show, for each wavelength (λ), the amplitude of mode induced by the incident combinations for the first n most aligned principle modes. For fields which obey Eq. (3), the internal and scattered modes can be independently addressed. Here we use two plane-polarized incident fields, either incident with their k-vector along the axis of the particle or at 60° to this direction. Figures a) and b) show the resulting internal amplitude for the two fields, while c) and d) are the scattered amplitudes. Both fields are linearly independent and both interact with the resonant feature at the back of the landscape (the fields also causes appreciable amplitude in several of the more poorly aligned modes further down the landscape). Figures e) and g) show the corresponding amplitudes for a field combination constructed to only cancel the internal component of the resonance (while leaving the scattered unchanged at the value caused by the axially incident light) for the resonant feature. f) and h) show the converse case of removing the amplitude of the resonance in the scattered space while leaving the internal unchanged. In both cases, the unchanged resonant mode is seem to retain exactly the same amplitude at its peak as the corresponding axial incident case; a) vs. f) and c) vs. g), whilst the paired mode in the other space is lost. Modes which are not controlled further down the landscape are also seen to acquire large amplitudes from these combinations of the incident field.

#192195 - $15.00 USD Received 12 Jun 2013; revised 9 Aug 2013; accepted 13 Aug 2013; published 22 Aug 2013

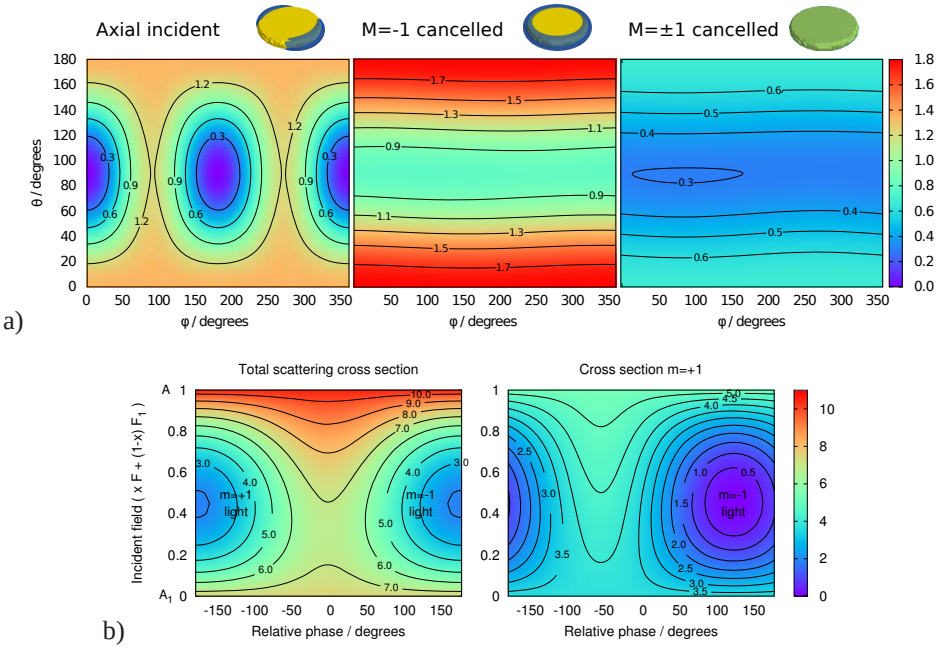

Fig. 4. Differential scattering for a rounded disc shaped (20 nm thickness and 60 nm radius) gold disc, with a dominant single pair mode modes showing a dipolar resonance at 697 nm (in a surrounding medium [19] with ε_r scaled by 0.75 to emulate support of the disc by a silica surface in air.) a) Scattering from an incident plane wave, with the square of the electric near field shown inset. This system clearly shows a dipole radiation pattern for axially incident light, which consists of light with both $m = \pm 1$ angular momentum. By introducing a second and then third field with chosen complex amplitudes, the light in the $m = -1$ and then both $m \pm 1$ channels can be removed, eventually leaving relatively little interaction with the incident light. b) Illustration of the effect of scanning for the condition to remove the $m = -1$ channel by adjusting the magnitude and phase of a second incident planewave. Experimentally, this example requires monitoring the orbital angular momentum of light emitted along the particle axis [20], to determine the relative amplitudes and phase where only the $m = -1$ dipolar resonance is active. Here we show the effect of scanning the relative amplitude and phase of light incident along the axis and an additional 45° direction (with respect to the particle axis) plane-polarized light. The scan is between the light consiting purely of the axially incident field A ($x = 1$) and field incident at 45° (A_1 at $x = 0$) and over the range of relative phases of the two incident light sources.

#192195 - $15.00 USD Received 12 Jun 2013; revised 9 Aug 2013; accepted 13 Aug 2013; published 22 Aug 2013

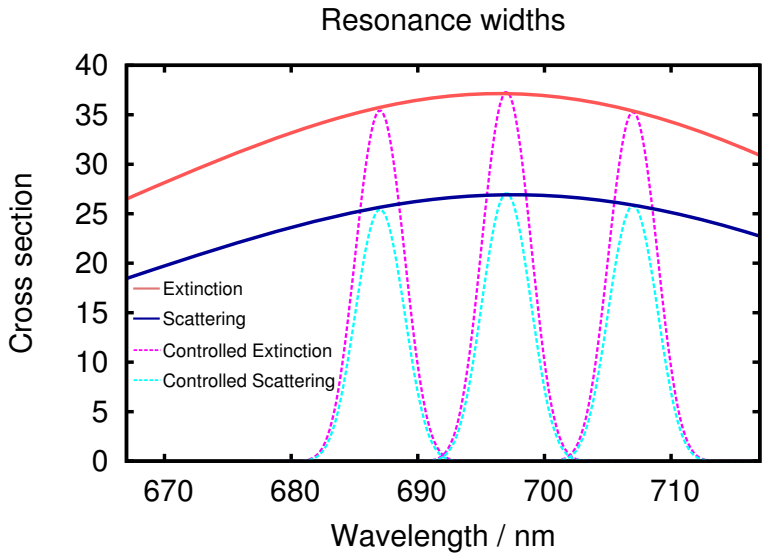

Fig. 5. Cross sections of the gold disc from Figure 4 with standard axial incidence, leading to a broad feature in the extinction (red) and scattering (blue). These are compared against its response to illumination of light from three directions (axial, 45 and 90° incident) with their relative phases (but not amplitudes) modulated to cause constructive interference only at a chosen wavelength, then rotating the phase to cause destructive interference according to a gaussian envelope, producing a specified location and line width feature within the envelope of the original broad peak.

Again using the spectral region around the resonance of the gold disc as an example, Fig. 5 shows an approach to produce sharper line widths of with a chosen line shape and peak position. Here, three incident fields have been chosen which cancel the resonance of the disc in both $m = \pm 1$ channels. These consist of axially incident plane wave light, light incident equatorially and light incident at 45 degrees to the particle axis. A combination of the three fields which do not produce amplitude in the principal modes of the the resonance were then constructed, chosen such that the equatorial light source amplitude was 1, and effectively removing interaction of these three light fields with the particle. Then, on scanning the wavelength of the light over the range, the phase (but not the amplitude) of the axial and 45 degree incident light was modulated according to a Gaussian profile, shifting their phase from being at the canceling combination to π out of phase with this over a narrow range of wavelengths. Figure 5 shows the results of choosing to remove the cancellation of the amplitudes at three different wavelengths. Equivalently different gaussian widths, or a different line profile could be chosen. Here, modulation of phase is being transferred into modulation of amplitude. This leads to a change between a situation similar to the final sub-figure of 4(a), when cancellation occurs, and a strong surface field and radiated light when the cancellation is disrupted. Experimentally, an approach similar to Fig. 1(b) may be able to produce the required change in phase of light over a narrow frequency range.

Conclusions

In conclusion we have shown that spatial distribution and angular momentum of internal and scattered fields of dielectric or metallic nanoparticles can be configured and optimized by con-

#192195 - $15.00 USD Received 12 Jun 2013; revised 9 Aug 2013; accepted 13 Aug 2013; published 22 Aug 2013

trolling the amplitudes of a finite number of internal and scattered modes of the nanoparticle through the relative phases of coherent sources of light. This can be achieved using a single source of light of the type normally available in experiments, beam splitters and phase modulators, or combination of internal and external sources. The number of sources required is equal to the number of channels to control plus one, so this general approach is particularly simple to implement near resonances, where the response to light of nanoparticles is dominated by few modes. We have also been able to use optical control to reshape the spectral response of nanoparticles, introducing narrow spectral lines of a few nanometers width. In general, the width of the narrow lines depends on the spectral resolution of the control set-up, i.e. of the gratings and of the diffractive elements used and can be much narrower than the resonance peaks of the nanoparticle. This can significantly improve the spectral resolution of surface enhanced spectroscopy, which is based on the enhancement of surface fields near nanoparticles. The same control approach can be applied to light generated through linear and nonlinear processes by impurities embedded in the particle. In this case, controlling internal modes allows one the management of non-linear transitions in the impurities. Most of all, the potential of this work lies in its generality and in the fact that it does not requires complex spatial shaping of the incident fields, but only the control of their relative phases and amplitudes that can be provided by already available diffractive elements such as spatial light modulators.

Appendix

In this section we review the principal mode theory, consider for which particles the internal and scattering modes can be controlled independently of one another and generalize the theory to the control of several modes. We consider metallic and dielectric particles without sharp edges and use [21] vectors, $F = [E,H]^T$, with three electric and three magnetic components for the electromagnetic fields; the corresponding surface field, f, consisting of the two electric and two magnetic components of F tangent to the surface of the particle. In this notation, the boundary conditions are $f = f^i - f^s$, i.e. the tangent components f of the incident field are equal to the difference between the tangent components of internal and scattered fields, f^i and f^s at the surface. We can find solutions of the Maxwell 's equation in the internal and external media, the principal modes I_n, S_n, such that the expansion of the scattered and internal fields converge to the exact fields for any incident field [22, 21, 10]. The tangent components of the principal modes, $\{i_n\}$ and $\{s_n\}$, form bases for the internal and scattered surface fields that are orthonormal with respect to the scalar product $f \cdot g = \sum_{j=1}^{4} \int_S f_j^* g_j d\sigma$, where j labels the components of the surface fields and the asterisk stands for the complex conjugate and $d\sigma$ is the infinitesimal surface area. Each pair i_n, s_n define an interaction channel for the particle that is independent from all the other pairs because each internal mode i_n is orthogonal to all but the scattering mode s_n and vice versa. The spatial correlations that appear in this theory can be interpreted geometrically. The principal cosine between s_n and i_n is defined by the overlap integral, or correlation [23], as $\cos(\xi_n) \equiv i_n \cdot s_n$, with the arbitrary phases of i_n, s_n chosen so that the integral is either positive or null. The corresponding function $\sin(\xi_n)$ is the orthogonal distance between s_n and i_n. The angles ξ_n characterize the geometry of the subspaces of the internal and scattered solutions and are invariant under unitary transformations [24]. Because of this property, the induced amplitudes of the n^{th} pair of principal modes of a nanostructure can be determined without need of noisy numerical inversion, by using the coupling of the surface projections of an incident field (f) to the internal (i_n) and scattered (s_n) mode pair as

$$a_n^i = \frac{i_n' \cdot f}{i_n' \cdot i_n},\ a_n^s = -\frac{s_n' \cdot f}{s_n' \cdot s_n}, \tag{6}$$

#192195 - $15.00 USD Received 12 Jun 2013; revised 9 Aug 2013; accepted 13 Aug 2013; published 22 Aug 2013

here, $g \cdot h$ indicates the surface integral of the scalar product of the projected fields, g and h. The sub-spaces of the internal and scattered modes are both orthonormal, i.e., $i_n \cdot i_m = s_n \cdot s_m = \delta_{nm}$ (with δ being the Kronecker delta), there are also associated *dual* biorthogonal modes:

$$i'_n = \frac{i_n - (i_n \cdot s_n)s_n}{\sqrt{1-(i_n \cdot s_n)^2}},\ s'_n = \frac{s_n - (i_n \cdot s_n)i_n}{\sqrt{1-(i_n \cdot s_n)^2}} \tag{7}$$

where $i'_n \cdot i'_m = s'_n \cdot s'_m = \delta_{nm}$, $i'_n \cdot s_n = s'_n \cdot i_n = 0$ and $i'_n \cdot i_n = s'_n \cdot s_n$. Note that in this work that i'_n and s'_n are chosen to be unit vectors, as distinct from [10]. From the denominator of Eq. (6), one can see [10] that large modal amplitudes can be achieved when the modes are strongly correlated, i.e., closely aligned. This mechanism is at the origin of resonances in nanoparticles as well as large transient gain and excess noise [25] in unstable optical cavities and classical or quantum systems governed by non-hermitian operators [26, 27].

Given the importance of spheres in scattering, we show explicitly how the optimization or suppression of either scattering or internal modes can be obtained when one source is internal and the other external, but not when both sources are either internal or external. The internal and scattering modes used in this work are proportional to the usual Mie modes: writing explicitly the electric and magnetic components, the magnetic multipole modes are defined, up to an arbitrary phase factor, as

$$i_{lm} = \frac{e^{i\phi_l}}{(|i_l^E(r)|^2 + |i_l^H(r)|^2)^{1/2}}[m_{lm}(\Omega)i_l^E(r), n_{lm}(\Omega)i_l^H(r)]^T, \tag{8}$$

$$s_{lm} = \frac{1}{(|s_l^E(r)|^2 + |s_l^H(r)|^2)^{1/2}}[m_{lm}(\Omega)s_l^E(r), n_{lm}(\Omega)s_l^H(r)]^T \tag{9}$$

where r is the radius of the sphere, Ω the solid angle, k_i, k are the wavenumbers for internal and external medium, respectively, m_{lm}, n_{lm} vector spherical harmonics. $i_l^E(r) = j_l(k_i r)$, $i_l^H(r) = -i(\varepsilon_i/\mu_i)^{1/2}(k_i r)^{-1}\partial_{k_i r} k_i r j_l(k_i r)$, $s_l^E(r) = h_l(kr)$, $s_l^H(r) = -i(\varepsilon/\mu)^{1/2}(kr)^{-1}\partial_{kr} krh_l(kr)$, j_l, h_l the spherical Bessel and Hankel functions of order l. $\phi_l = -Im\{\log[i_l^E(r)^* s_l^E(r) + i_l^H(r)^* s_l^H(r)]\}$ is such that

$$i_{lm} \cdot s_{lm} = \frac{|i_l^E(r)^* s_l^E(r) + i_l^H(r)^* s_l^H(r)|}{(|i_l^E(r)|^2 + |i_l^H(r)|^2)^{1/2}(|s_l^E(r)|^2 + |s_l^H(r)|^2)^{1/2}}. \tag{10}$$

Electric multipole modes are obtained as usual exchanging magnetic with electric parts. The incident fields generated by two external sources can be expanded in terms of electric and magnetic multipoles centered on the sphere; the only terms of these expansions that can couple to the modes in Eqs. (8, 9) are $f = a[m_{lm}(\Omega) f_l^E(kr), n_{lm}(\Omega) f_l^H(kr)]^T$, $f^1 = a_1[m_{lm}(\Omega) f_l^E(kr), n_{lm}(\Omega) f_l^H(kr)]^T$, where $f_l^E(kr), f_l^H(kr)$ are found by replacing $k_i r$ with kr in i_l^E, i_l^H . Therefore we find that both terms in Eq. (3) are equal to a/a_1, i.e. the inequality is violated. On the contrary, the equality can be satisfied when the two sources are such that $f_l^{1E} \neq f_l^E, f_l^{1H} \neq f_l^H$. This is the case when one source is external and the other is a radiating multipole inside the particle with $f^1 = a_1[m_{lm}(\Omega) f_l^{1E}(k_i r), n_{lm}(\Omega) f_l^{1H}(k_i r)]^T$, where $f_l^{1E}(k_i r), f_l^{1H}(k_i r)$ are found by replacing kr with $k_i r$ in s_l^E, s_l^H. For this combination of internal and external sources Eqs. (4, 5), for suppression of i_{lm} and maximal excitation of s_{lm}, can be applied and are

$$A_1 = -A\frac{f_l^{E*} i_l^E + f_l^{H*} i_l^H}{f_l^{1E*} i_l^E + f_l^{1H*} i_l^H}, \tag{11}$$

$$A_1 = -A\frac{f_l^{E*}(e^{i\phi_l} i_l^E - \cos(\xi_n) s_l^E) + f_l^{H*}(e^{i\phi_l} i_l^H - \cos(\xi_n) s_l^E)}{f_l^{1E*}(e^{i\phi_l} i_l^E - \cos(\xi_n) s_l^E) + f_l^{1H*}(e^{i\phi_l} i_l^H - \cos(\xi_n) s_l^E)}. \tag{12}$$

#192195 - $15.00 USD Received 12 Jun 2013; revised 9 Aug 2013; accepted 13 Aug 2013; published 22 Aug 2013

The same analysis holds true also for infinite cylinders.

We consider now an incident field generated by external source with $f_n \neq 0$, $f_{n_\perp} = 0$. i_n, s_n, f_n are exact solutions of the Maxwell's equations that, for particles with continuously varying surface tangents (particles of class C^1), have Stratton-Chu representation [18]

$$\int [i\omega\mu(n \times S_n^H) - \nabla \times (n \times S_n^E) - \nabla(n \cdot S_n^E)] g(x,y) d\sigma = 0 \quad (13)$$

$$\int [i\omega\mu(n \times F_n^H) - \nabla \times (n \times F_n^E) - \nabla(n \cdot F_n^E)] g(x,y) d\sigma = -F_n^E(x), \quad (14)$$

with μ the magnetic permitivity of the external medium, ω the frequency of light, the outgoing normal, n, the fields F, S and the infinitesimal area $d\sigma$ depend on a point y on the surface of the particle, x is a point inside the particle, ∇ acts on x and $g(x,y,k)$ is the Green function of the scalar Helmholtz equation for the external medium [28]. For x infinitesimally close to the surface, using Eq. (13) and the boundary conditions in Eq. (14) and the conservation of energy we get

$$-n(x) \times \left(n(x) \times \int \left[i\omega\mu(n \times I_n^H) - \nabla \times (n \times I_n^E) - \frac{\varepsilon_i}{\varepsilon} \nabla(n \cdot I_n^E) \right] g(x,y) d\sigma \right) = \frac{a_n^s}{a_n^i} s_n(x) - i_n(x) \quad (15)$$

$$W_n = |a_n^i|^2 W_n^i - |a_n^s|^2 W_n^s + \frac{1}{2} Re \left[\int n \cdot (a_n^i a^{s*}{}_n i_n^E \times s_n^{H*} + a^{i*}{}_n a_n^s s_n^E \times i_n^{H*}) d\sigma \right] = 0, \quad (16)$$

where $\varepsilon_i, \varepsilon$ are the dielectric constant of the internal and external media and W_n, W_n^i, W_n^s are the power fluxes of f_n, i_n, s_n [28]. Eq. (15) and its magnetic equivalent are independent complex equations that must be solved up to a factor by a_n^i, a_n^s ; because a_n^i, a_n^s do not depend on x, these equations can be solved only if the dependence on x in all the terms in Eq. (14) can be factored out. When this happens, as for spheres and cylinders, Eq. (16) shows that the condition in Eq. (3) cannot be satisfied by incident fields generated by sources outside the particle.

Finally, the procedure in Eq. (4) is can be generalized fixing, for instance, the amplitude of one mode, say $a_1^i = c$, and setting to zero the amplitudes of m internal modes and l scattering modes using $m + l + 2$ incident fields that satisfy the following equation

$$\begin{bmatrix} \frac{i_1' \cdot f^1}{\sin(\xi_1)} & \cdots & \frac{i_1' \cdot f^{m+l+1}}{\sin(\xi_1)} \\ \vdots & & \vdots \\ \frac{s_l' \cdot f^1}{\sin(\xi_l)} & \cdots & \frac{s_l' \cdot f^{m+l+1}}{\sin(\xi_l)} \end{bmatrix} \begin{bmatrix} A_1 \\ \vdots \\ A_{m+l+1} \end{bmatrix} = - \begin{bmatrix} A \frac{i_1' \cdot f}{\sin(\xi_1)} - c \\ A \frac{i_2' \cdot f}{\sin(\xi_2)} \\ \vdots \\ A \frac{s_l' \cdot f}{\sin(\xi_l)} \end{bmatrix}. \quad (17)$$

where $f^1, \ldots, f^{m+l+1}$ are arbitrary. The solution for the amplitudes $A^1, \ldots, A^{m+l+1}$ is unique if the determinant of the matrix is not null.

#192195 - $15.00 USD Received 12 Jun 2013; revised 9 Aug 2013; accepted 13 Aug 2013; published 22 Aug 2013